Biosensors and Bioelectronics 142 (2019) 111531

Contents lists available at ScienceDirect

Biosensors and Bioelectronics

journal homepage: www.elsevier.com/locate/bios

A label-free electrochemical biosensor for highly sensitive detection of gliotoxin based on DNA nanostructure/MXene nanocomplexes

Hui Wang[a], Hui Li[a], Yue Huang[b], Menghua Xiong[c], Feng Wang[a,**], Chao Li[a,*]

[a] School of Food and Biological Engineering, Hefei University of Technology, Hefei, 230009, PR China
[b] Department of Food Science and Engineering, College of Light Industry and Food Engineering, Nanjing Forestry University, Nanjing, 210037, PR China
[c] Institutes for Life Sciences, South China University of Technology, Guangzhou, 510006, PR China

ARTICLE INFO

Keywords:
DNA nanostructure
Electrochemical biosensor
Mycotoxin detection
MXene

ABSTRACT

The use of new functional two-dimensional nanomaterials for construction of advanced biosensors has attracted great attention. Herein, we report an electrochemical DNA (E-DNA) biosensor to detect gliotoxin based on DNA nanostructure-modified MXene (Ti_3C_2) nanosheets. Tetrahedral DNA nanostructures (TDNs) were facilely immobilized onto the surface of MXene nanosheets through coordination interactions between the phosphate groups on DNA and titanium, which avoids cumbersome and expensive modification of DNA probes. MXene nanosheets possess large surface area to modify a large number of DNA probes and excellent conductivity to facilitate the electron transfer between electrochemical species and the underlying electrode surface. Meanwhile, the unique configuration of TDN enables efficient and rapid binding of target molecules onto electrode surface, thereby producing amplified electrochemical signals. Through combining the merits of the two nanomaterials, the proposed sensor exhibits a wide detection range from 5 pM to 10 nM with a low limit of detection (LOD) of 5 pM. We believe that this work opens a new avenue for development of MXene-based E-DNA biosensors and could be further extended to detect other mycotoxins.

1. Introduction

In the past decade, two-dimensional (2D) nanomaterials have received much attention in the development of electrochemical biosensing devices due to their impressive physiochemical properties (Campuzano et al., 2017; Peng et al. 2018, 2019; Song et al., 2016; Tiwari et al., 2016). As the pioneering 2D nanomaterial, graphene oxide (GO) is the most extensively used one in the biological applications due to its ultrathin structure, hydrophilicity and biocompatibility, but the defects and abundant oxygenic groups on the GO plane result in poor electronic conductivity and thereby restrict its direct application in electrochemistry(Liu et al., 2019). Therefore, the conversion of GO to reduced GO (rGO) with good conductivity is essential for most of electrochemical biosensors, but the low solubility and reduced functional groups make rGO easy to aggregate and difficulty to bio-functionalization, limiting its further application in bioanalysis.

Recently, a new class of 2D layered material composed of transition metal carbides, nitrides, and carbonitrides known as MXenes, has emerged(Eklund et al., 2017; Novoselov et al., 2004). The 2D layered MXene nanosheets are obtained through selectively removing “A” layers from bulky $M_{n+1}AX_n$ phases, where M is an early transition metal, A represents an A-group mostly from groups 13 and 14 of a periodic table, and X represents C and/or N (n = 1–3), leading to a general formula of $M_{n+1}X_n$(Naguib and Gogotsi, 2014). Since the MXene nanosheets have abundant surface functional groups, such as –O, –OH, and –F, which allow them to dissolve in a wide range of solvents, including water and strong polar organic solvents (e.g., ethanol, dimethyl sulfoxide, and acetone, etc.) At the same time, because of their high metallic properties, MXenes exhibit good electrical conductivity (2400 S/cm) which favors their potential application in electrochemistry(Dillon et al., 2016; Sang et al., 2016). Hence, MXenes have an advantageous combination of GO and rGO's characters, and they are widely studied in the fields of supercapacitor(Wen et al., 2017), oxygen-evolution reaction(Gao et al., 2016) and battery(Er et al., 2014). Quite recently, some electrochemical biosensors based on MXene nanosheets have also been developed. For example, Chen and co-workers took advantage of MXene as a robust matrix to immobilize tyrosinase for mediator-free detection of phenol(Wu et al., 2018). Salama and colleagues reported aminosilane-functionalized MXene nanosheets to anchor antibodies and used them for electrochemical

* Corresponding author.,
** Corresponding author.
E-mail addresses: fengw420@hfut.edu.cn (F. Wang), lchao@hfut.edu.cn, Biosensorli@yeah.net (C. Li).

https://doi.org/10.1016/j.bios.2019.111531
Received 14 May 2019; Received in revised form 3 July 2019; Accepted 21 July 2019
Available online 25 July 2019
0956-5663/

detection of cancer biomarker(Kumar et al., 2018). However, most of the studies focus on the immobilization of enzyme or protein molecules onto MXene nanosheets and make functional enzyme electrodes(Sinha et al., 2018), and the employment of DNA nanostructure (DN) and MXene to develop electrochemical DNA (E-DNA) sensors for ultrasensitive detection of biomolecules is still unexplored.

Generally, E-DNA sensors using DNs as interfacial probes possess superior analytical performance compared to traditional sensors using single-stranded DNA (ssDNA) or double-stranded DNA (dsDNA) probes in terms of sensitivity, selectivity and reproducibility (Huang et al., 2018; Yang et al., 2018); however, one major limitation of these biosensors is the high cost for synthesis of DNs that usually need cumbersome modification. For example, the most popular used DN, namely tetrahedral DNA nanostructure (TDN), usually needs three thiol groups and one molecular linker (e.g., biotin), significantly increasing reagent cost and synthesis difficulty. For 2D nanomaterials' functionalization, noncovalent adsorption is the most popular way for low-cost conjugation of DNA probes through its nucleobases to π–π stacking and hydrogen bond with 2D nanomaterials (e.g., GO). Nevertheless, these physiosorbed DNA probes often lie flat on the surface of 2D nanomaterials and easily detach from the surface by nonspecific competitive substitution (e.g., proteins), leading to low recognition capability and false positive signals(Liu et al., 2018).

Herein, we prepare TDN modified MXenes and make use of them as novel interfacial probes for sensing gliotoxin, one of the most toxic metabolites produced during the growth of Aspergillus fumigatus (Brown et al., 2012), which poses a serious threat to the health of humans and animals. Since phosphate is abundant in nucleic acid but not in proteins, nanomaterials binding with phosphate can better recognize DNA from most protein interferents in the complex matrix (e.g., serum). Considering the basal plane of MXenes is abundant of transition metal (e.g., titanium), we hypothesized that the TDNs might be facilely adsorbed onto the MXene surface via strong chelation interaction between titanium and phosphate groups. Therefore, an electrochemical biosensor with several advantages could be envisioned. First, MXene nanosheets provide ample space for the adsorption of numerous TDNs and an electroactive surface for signal transduction. Second, titanium element on the surface of MXene nanosheets offers a facile method for assembly of TDNs with phosphate backbone, which does not involve cost and complex chemical modification of TDNs. Third, TDNs are served as rigid scaffolds to keep their appropriate orientation and facilitate molecular recognition on the electrode surface, thereby producing amplified signal. Finally, the use of another functional nucleic acid, i.e., gliotoxin aptamer(Gao et al., 2019), also allows efficient recognition of analytes in a cost-effective manner. To our best knowledge, this is the first example that combined use of MXene and TDNs to develop an electrochemical biosensor for mycotoxin detection. The present work thus demonstrates the promising application of MXene and DNs in the development of highly sensitive, cost-effective and environmentally friendly electrochemical biosensors.

2. Experimental section

2.1. Chemicals and materials

All DNA strands (Table S1) were purchased from Sangon Biotech Co., Ltd (Shanghai, China) and purified by high-performance liquid chromatography (HPLC). Gliotoxin was obtained from Biopurify Phytochemicals Ltd. (Chengdu, China). Bovine serum albumin (BSA), and ultrasensitive streptavidin-peroxidase polymer were purchased from Sigma-Aldrich (St. Louis, MO, U.S.A.). A ready-to-use TMB solution (TMB = 3, 3′, 5, 5' tetramethylbenzidine) was ordered from Neogen (K-blue low activity substrate, H_2O_2 included). All other chemicals were of analytical grade and were used without further purification.

Healthy human serum samples were collected from volunteers from our labs. Collected blood samples were centrifuged at 1700 *g* for 10 min at 4 °C, and supernatant plasma was carefully transferred into new tubes followed by another centrifugation at 1700*g* for 10 min at 4 °C.

The buffers and solutions involved in this work were as follows: TDN preparation (50 mM Tris-HCl containing 10 mM $MgCl_2$, pH 7.4), incubation buffer (50 mM Tris-HCl containing 100 mM NaCl, 1 mM $MgCl_2$ and 1 mM $CaCl_2$, pH 7.4), washing buffer (0.02 M phosphate buffer saline (PBS) containing 0.5 M NaCl, 0.1% BSA), and detection buffers (ready-to-use TMB solution).

2.2. Apparatus

All electrochemical experiments were conducted using CHI 660E workstation (Shanghai CH Instruments Co. Ltd, China). A conventional three-electrode system was used, where glassy carbon electrode or gold electrode (2 mm in diameter) was employed as the working electrode, a platinum wire as the counter electrode, and the reference electrode was Ag/AgCl (3 M KCl). Cyclic voltammetry (CV) was recorded with a scan rate of 100 mV/s. The *I*-t curves were detected at −0.1 V and the electrocatalytic current was recorded at 60 s after the HRP redox reaction reached the steady state. Electrochemical impedance spectroscopy (EIS) measurements were conducted in 5.0 mM $[Fe(CN)_6]^{3-/4-}$ solution containing 0.1 M KCl.

Atomic force microscopy (AFM) characterization was recorded on a Bruker Multimode 8 (Bruker, America) with tapping mode. Dynamic light scattering (DLS) was measured by Malvern Nano ZS system. Transmission electron microscopy (TEM) was performed with a JEOL model 2000 instrument. Scanning electron microscopy (SEM) was performed with a Hitachi SU8020 instrument. The nanomaterial was characterized by a powder X-ray diffraction system (XRD, Bruker, D8 ADVANCE) equipped with Cu Kα radiation. The UV–vis absorption spectra were recorded on a photospectrometer (PerkinElmer, Lambda 465) at room temperature. Dynamic light scattering (DLS) and zeta potential analysis of Au NPs were performed on a Zeta Sizer Nano ZS (Brookhaven Instruments Ltd.).

2.3. Nanomaterials preparation

MXene nanosheets were synthesized according to previous reports (Han et al., 2018). Briefly, Ti_3AlC_2 power (5 g) was etching with 40 mL 40% HF at room temperature for 3 daysat room temperature to remove the Al layer. After centrifugation with the washing by ethanol and water for three times, the samples were added into 25 wt% tetrapropylammonium hydroxide (TAPOH) aqueous solution and stirred for 72 h. After centrifugation to remove TPAOH, the precipitate was dispersed into water and sonicated for 2 h, followed by centrifugation (3000 rpm). Finally, the supernatant was the exfoliated MXenes two-dimensional nanomaterials and was stored under 4 °C.

TDN probe was synthesized based on our previous reports(Li et al., 2018; Yang et al., 2019). Briefly, equal quantities (10 μM) of four strands (TDN1-4) were mixed and then heated to 95 °C for 5 min and immediately cooled to 4 °C. Then, the TDN probe could be diluted in incubation buffer for subsequent application.

2.4. Adsorption of TDNs in TDN/MXene complex

A 10 μL volume of an aqueous solution of MXene (5 mg/mL) was added to 90 μL of an aqueous solution containing 2.5 μM TDN in PCR tubes. After vortexing for 10 s, the mixture was incubated at room temperature for 1 h. The resulting complex was centrifugated and the precipitation was dispersed and stored at 4 °C for subsequent use.

2.5. Sensor fabrication

Prior to sensor fabrication, a bare glassy carbon electrode (GCE, diameter 0.2 cm) was polished with 1000 nm, 300 nm and 50 nm

alumina slurries in sequence, and then ultrasonically washed in ethanol and ultrapure water. Then, the electrodes were subjected to electrochemical cleaning in H_2SO_4 solution. Simultaneously, the TDN/MXene complex was sonicated in 0.5% Nafion solution to get a concentration of 0.05 mg/mL 5 μL of the suspension was then film cast onto the surface of the GCE and allowed to dry slowly. After immobilization, the blank sites on the electrode was then blocked with 1% BSA at room temperature for 2 h. Then, the obtained GCEs were coated with an extra 2 μL layer of 0.5% Nafion. The electrodes were rinsed with washing buffer and stored in the buffer at 4 °C prior to use. According to the equation for a reversible process (Wang et al., 2007), the real surface area of the electrode of a bare GCE and a TDN/MXene-GCE can be calculated to be 0.0411 cm^2 and 0.124 cm^2, respectively. The modified electrode increased in area by nearly 201%.

Different concentrations (9 μL) of the target were mixed with aptamer/signal probe (1 μL, 100 nM) and then incubated on the surface of electrode at room temperature for 0.5 h. After rinsing, 5 μL of ultrasensitive streptavidin-peroxidase polymer (10^3 dilution with PBS) was dropped onto the electrode surface for 15 min incubation at room temperature. Finally, the sensor was then thoroughly washed with buffer and subjected to electrochemical measurements.

3. Results and discussion

3.1. Sensor principle

As shown in Scheme 1, the main working principle of the electrochemical biosensor is presented. The four vertexes of the TDN probe are extended upon one identical capture strand, respectively. Since the TDN is high rigid and symmetrical, at least one capture strand will be consistently exposed into solution regardless of its configuration on the surface of MXene. This 3D complex probes avoids the probes of "lying-down" posture because of the steric hindrance, which favors analytical recognition. The TDN/MXene complex can be simply prepared by mixing the two nanomaterials and then dropped onto the electrode surface (Scheme 1). In the presence of gliotoxin, the aptamer-analyte binding is competitive with the hybridization of aptamer and its complementary strand (i.e., signal probe). The released signal probes are easily captured by TDN probes and the included streptavidin-targeting aptamer (green loop) will pull streptavidin-labeled horseradish peroxidase (HRP) down to electrode surface, producing large catalytic current signal.

3.2. Characterization of MXene and TDN

Ultrathin MXene (Ti_3C_2) nanosheets were synthesized through a two-step exfoliation methodology from the bulk layer-structured Ti_3AlC_2 MAX-phase ceramic. The successful HF etching and exfoliation of Ti_3AlC_2 MAX-phase ceramic was demonstrated through scanning electron microscopy (SEM) and X-ray diffraction (XRD) (Fig. S1). . Transmission electron microscopy (TEM) revealed the successful production of MXene nanosheets (Fig. 1A). The UV–vis absorption spectrum of MXene nanosheets in water (Fig. 1B) displaced a big peak around 280 nm and the typical absorption ranging from 750 to 850 nm, which was due to their interband transitions(Yu et al., 2017).

TDN probes were prepared by one-step annealing. Different techniques, including gel electrophoresis, dynamic light scatting (DLS), and atomic force microscopy (AFM), were used to demonstrate the successful synthesis of TDN (Fig. S2).

3.3. The interaction between TDN and MXene

The interaction between TDN and MXene was first tested by UV–vis spectroscopy. As shown in Fig. 2A, the as-synthesized TDN has a typical characteristic peak at 260 nm. After incubation with MXene and subsequent centrifugation, the absorbance of 260 nm of the supernatant dramatically reduced, suggesting the adsorption of TDN onto MXene nanosheets. The adsorption efficiency of TDN was calculated to be as high as 86.2%. Then, fluorescence was also employed investigate the interaction between TDN and MXene through labeling TDN with a fluorophore (i.e., FAM), since MXene could efficiently quench the fluorescence of FAM if the TDN is adsorbed onto the surface of MXene. Fig. 2B showed that the adsorption of TDN onto MXene nanosheets was very fast and the most of adsorption could be completed within 1 min. Of note, the adsorbed TDNs were only replaced by high concentration of phosphates and were not affected by other interferents such as

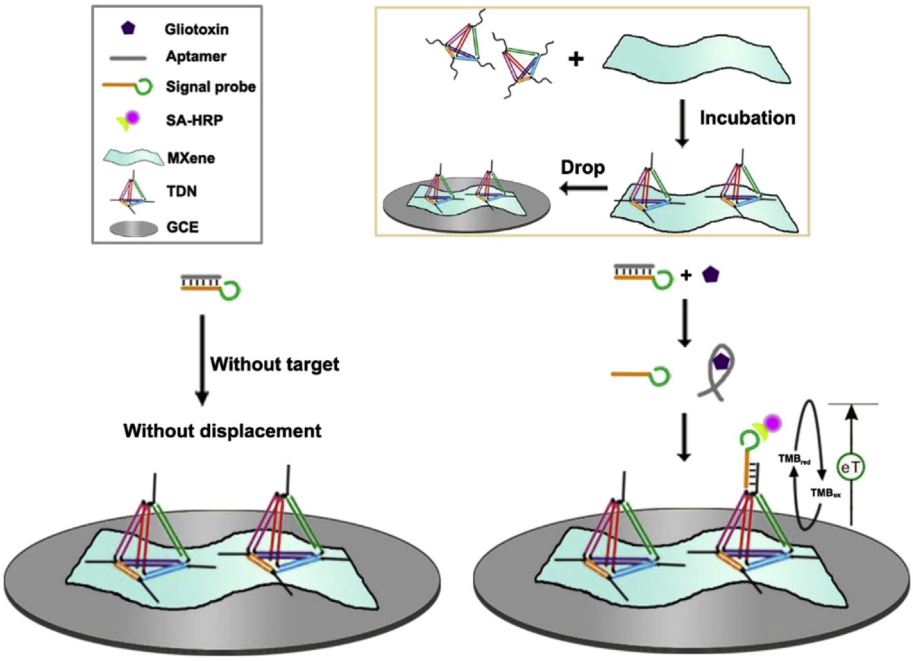

Scheme 1. Schematic illustration of the preparation of TDN/MXene modified electrode and the principle of TDN/MXene-based electrochemical sensor for gliotoxin detection.

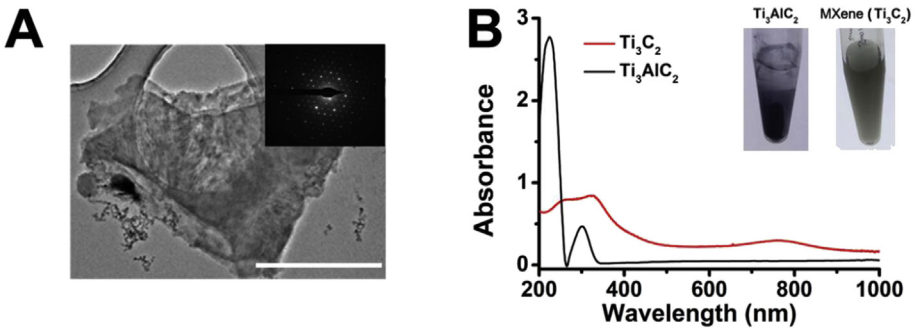

Fig. 1. Characterization of the MXene (Ti_3C_2) nanosheets. (A) TEM image of the as-synthesized MXene (Ti_3C_2) nanosheets. Scale: 1 μm. Inset: image of the selected-area electron diffraction (SAED) of MXene. (B) UV–vis spectra of Ti_3AlC_2 solution (black curve) and MXene (Ti_3C_2) nanosheets (red curve). Inset: photographic of Ti_3AlC_2 solution (left) and MXene (Ti_3C_2) solution (right). (For interpretation of the references to colour in this figure legend, the reader is referred to the Web version of this article.)

protein and salt (Fig. S3), implying their robust interaction and potential application in complex matrix. Then, DLS was used to investigate the size change before and after immobilization of TDN (Fig. 2C). The addition of TDN decreased the size of MXene nanosheets, indicating the increased stability of the MXene nanosheets in the solution. This is probably due to the introduction of highly negatively charged DNA nanostructure onto MXene surface increased electrostatic repulsion and inhibited the interaction between different MXene layers. Finally, AFM was utilized to confirm the adsorption of TDN onto the surface of MXene nanosheets (Fig. 2D). The thickness of the MXene was about 2.3 nm, which indicated that they were mainly comprised of a single layer. After incubation with TDN, many small dots appeared on the surface of MXene nanosheets, suggesting the interaction between TDN and MXene nanosheets. Also of note, the height of TDN probes on the MXene surface was approximately 3.1 nm, indicating they keep upright configurations on the surface due to the highly rigid stereostructure. Meanwhile, TDN structures critically increase the vertical distance between the capture strands and the MXene surface, and thus provide the molecular recognition a necessary bulk-solution-like phase.

3.4. Electrochemical characteristic of TDN/MXene functionalized electrode

Electrochemical impedance spectroscopy (EIS) is a useful technique to characterize the electronic transfer properties of the electrodes. Fig. 3A showed the EIS diagrams of different modified electrodes. Relative to bare GCE (black curve), modification of MXene nanosheets resulted in a reduced R_{ct} (red curve). This should be attributed to the high surface area and excellent metallic conductivity of MXene. The direct assembly of TDNs onto the electrode surface significantly hindered the electron transfer (blue curve), owing to electrostatic repulsion between $Fe(CN)_6^{3-/4-}$ and the negatively charged phosphate backbones of TDNs. However, once introduction of TDN/MXene complex (pink curve), the R_{ct} was much smaller than that of TDN-modified electrode surface, implying the good conductivity of the MXene.

To test the feasibility of the proposed sensor, we employed the *I*-t curve to determine the amperometric responses under different conditions. Fig. 3B showed that the sensor produced a large cathodic current of 1180 nA when gliotoxin of 10 nM was added (orange curve). In the absence of gliotoxin, however, a relatively large background signal was observed (red curve, ~326 nA), which was probably owing to the nonspecific adsorption of signal probe/aptamer duplex or enzyme. So, bovine serum albumin (BSA) was introduced to block the unoccupied

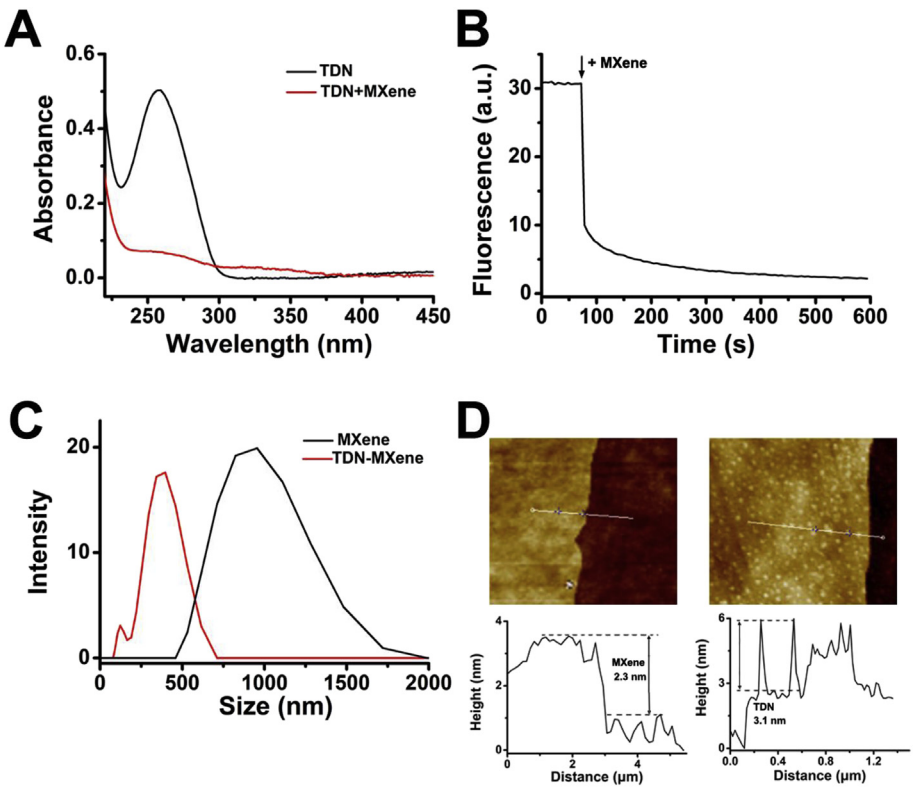

Fig. 2. (A) UV–vis spectra of TDN (black curve) and the supernatant of TDN after addition of MXene and centrifugation (red curve). (B) Kinetic study of the adsorption of TDN onto MXene nanosheets. [TDN] = 10 nM and [MXene] = 0.01 mg/mL (C) DLS results of the MXene nanosheets before (black curve) and after (red curve) addition of TDN. (D) AFM images of the MXene nanosheets before (left) and after (right) addition of TDN. The appearance of small dots on the MXene nanosheet indicates the adsorption of TDN probes. (For interpretation of the references to colour in this figure legend, the reader is referred to the Web version of this article.)

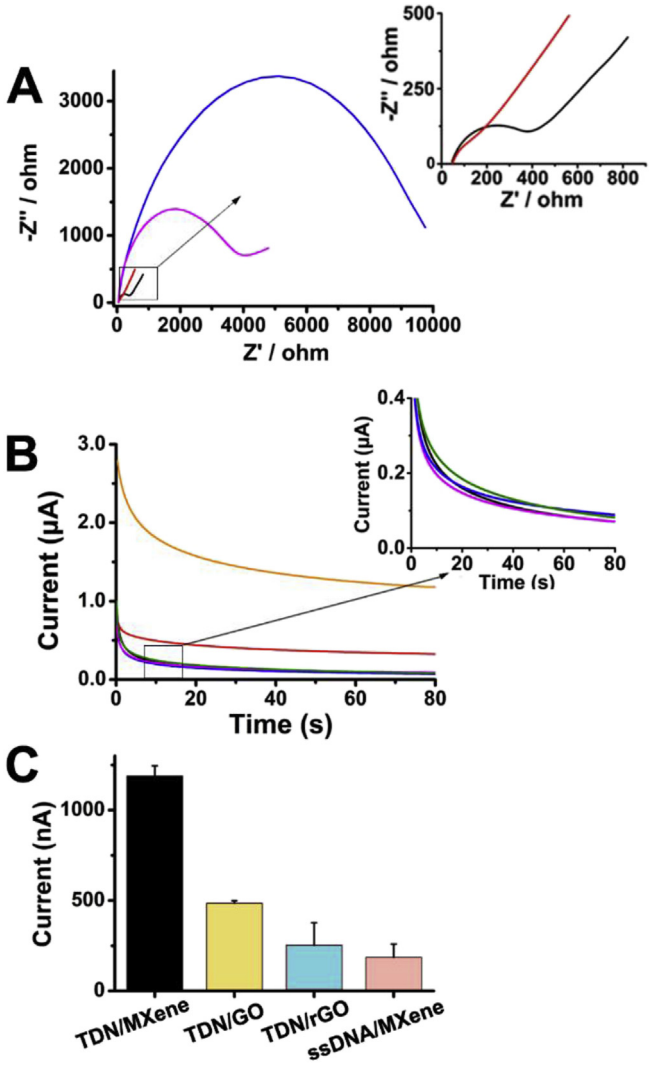

Fig. 3. (A) Nyquist plots of bare GCE (black curve), MXene-GCE (red curve), TDN-GCE (blue curve), and TDN/MXene/GCE (pink curve) in 5 mM $K_3[Fe(CN)_6]/K_4[Fe(CN)_6]$ (1:1) containing 0.5 M KCl. Insert: Amplified Nyquist plot of bare GCE and MXene-GCE. (B) *I*-t curves of the sensor under different conditions. Orange curve: 10 nM target; black curve: blank control with backfilling; red curve: blank control without backfilling; green curve: aptamer replaced by random sequence; pink curve: capture strand replaced by random sequence in TDN probe; blue curve: signal strand without SA aptamer. Inset shows the zoom-in view at low current. (C) Comparative study of the TDN/MXene sensor with other control sensors including TDN/GO sensor, TDN/rGO sensor and ssDNA/MXene sensor. (For interpretation of the references to colour in this figure legend, the reader is referred to the Web version of this article.)

space of TDN/MXene complex and electrode. After appropriate blocking, the background signal was successfully suppressed (black curve, 70 nA). Several control experiments were also conducted to further validate the sensor. For example, when the aptamer, the SA aptamer in signal probe, or capture probe in TDN was replaced by a random sequence, respectively, there was no obvious current change (blue, green, and pink curve, respectively), further confirming the indispensable role of the three functional elements in the probe.

To emphasize the advantage of MXene, we prepared control electrochemical biosensors using GO or rGO to replace MXene. As shown in Fig. 3C, the GO-based sensor generated a rather moderate current signal (485 nA) when challenged with 10 nM target, which may be due to the poor conductivity of the GO (Fig. S4). Although rGO has good conductivity, it was difficult to obtain a homogeneous solution of rGO (Fig. S5), so the loading rate of TDN is low (about 28.4%), thereby leading to low signal generation (~253 nA). Furthermore, in order to ascertain the advantage of TDN probe, we also prepared ssDNA-MXene complex modified electrode. Without 3D nanostructure, the recognition efficiency of ssDNA probes on the MXene nanosheets is rather low and the electrochemical response (~186 nA) was much weaker than its TDN/MXene-based counterpart. These results demonstrated the TDN/MXene-based sensors had better molecule recognition ability.

3.5. Optimization of experimental parameters

The concentration of TDN/MXene complex is first investigated. As shown in Fig. S6A, with increase the TDN/MXene complex concentration from 0.01 to 0.2 mg/mL, the amperometric value kept increasing until 0.05 mg/mL, indicating that 0.05 mg/mL of TDN/MXene coating is already enough and saturated for signal probe binding. Therefore, a concentration of 0.05 mg/mL of TDN/MXene complex was chosen to modify the electrode. The concentration of blocking reagent (i.e., BSA) was also evaluated. Fig. S6B exhibited that the control group showed false-positive results before 1% BSA, which was probably owing to the fact that the insufficient blocking reagent led to nonspecific interaction of the signal probe or enzyme. Therefore, 1% of BSA was selected as the appropriate concentration of blocking reagent. The length of signal probe had large effect on the sensor performance, which is essential to the hybridization between signal probe and aptamer or TDN. We tested the signal probe with lengths ranging from 12 to 20 nucleotides (Fig. S6C). The amperometric signal of experiment group gradually increased with the lengths of signal probe ranging from 12 to 14 nucleotides; however, when the nucleotides were longer than 14 nucleotides, i.e., 17 and 21 nucleotides, the decline of current signal might be attributed to the low displacement efficiency of target toward signal probe/aptamer duplex. Thus, the length of the signal probe was chosen as 14 nucleotides in this method. In addition, with the increase of pH, the current signal increased rapidly and then decreases (Fig. S6D). The highest response can be obtained at pH value from 6.0 to 8.0, coincident with the pH of commonly used buffer solutions. Furthermore, these experimental results indicate that the proposed sensor could work well in a wide range of pH.

3.6. Analytical performance of the proposed sensor

The ability of the proposed sensor for quantitatively detection of gliotoxin was evaluated. Fig. 4A showed typical *I*-t decay curves at −0.1 V toward gliotoxin at varying concentrations, which reaches a plateau within 80 s. The current was continually increasing as the concentration of gliotoxin increased from 5 pM to 10 nM. The plot of amperometric responses (I) versus the concentration of gliotoxin as depicted Fig. 4B, and the amperometric response reached a plateau point at 50 nM of gliotoxin. The detection of limit (LOD) was as few as 5 pM, which could be estimated as the lowest detected concentration whose signal was higher than the threshold equal to background signal plus three standard deviations. As shown in Table 1, in contrast to other reported methods, the proposed assay using MXenes and TDN showed enhanced performance. Also of note, compared with previous TDN-based electrochemical sensor, the probe cost was dramatically reduced from around 121 $/OD to 26 $/OD (Table S2), which was highly desirable for its scalable application.

To investigate the specificity, ochratoxin A (OTA), aflatoxin B1 (AFB1), adenosine triphosphate (ATP) and bovine serum albumin (BSA), (100 nM, respectively) were chosen as controls, whose concentration was 10-fold relative to the concentration of gliotoxin (10 nM). As shown in Fig. 4C, compared with the blank control, no obvious amperometric responses from controls were observed except that of gliotoxin. These results suggested good specificity of this assay for gliotoxin detection, which is attributed to the high selectivity of the used aptamer toward gliotoxin.

To further explore its potential in real application, the biosensor was

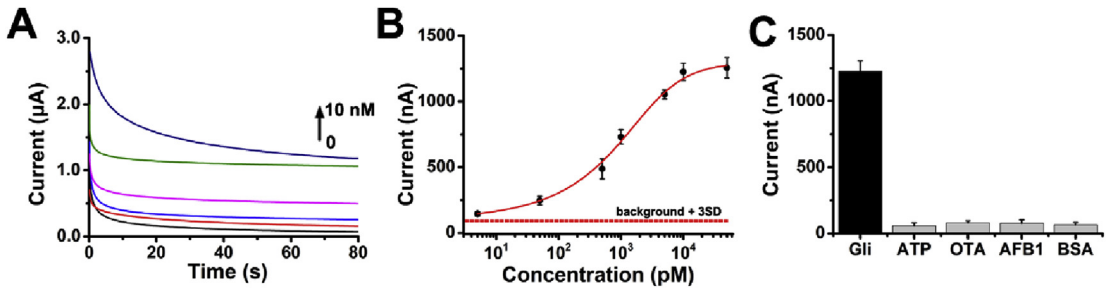

Fig. 4. Electrochemical performances of the proposed sensor for gliotoxin detection. (A) Amperometric curves for the detection of gliotoxin at a series of concentrations (from bottom to top: 0, 5, 50, 500, 5000, and 10000 pM). (B) Logarithmic plot of amperometric current versus gliotoxin concentration. The dash line (red) represents the threshold (background signal + 3 standard derivations). Error bars represent standard deviations for measurements taken from six independent experiments. (C) Specificity of the proposed sensor for detection of gliotoxin (10 nM) and other interferents (100 nM). (For interpretation of the references to colour in this figure legend, the reader is referred to the Web version of this article.)

Table 1
Performance comparison toward gliotoxin detection with other methods.

Method	LOD	Detection range	Reference
LC-MS-MS	Not reported	0.25–25 ng/mL	Lewis et al. (2005a)
Bioassay	20 ng/well	0.2–1 μg/mL	Grovel et al. (2006)
HPLC-MS/MS	3 ng/mL	10–120 ng/mL	Cerqueira et al. (2014)
HPLC	25 ng/mL	25–1000 ng/mL	(Lewis et al., 2005b)
Fluorescence	0.016 ng/mL	0.03–32.6 ng/mL	Gao et al. (2019)
Electrochemistry	1.63 pg/mL	1.63–3260 pg/mL	This work

challenged with complex samples. Human serum samples were spiked with free gliotoxin at different concentrations. As shown in Table S3, the recovery ranged from 96.3% to 115% and low relative standard deviations (RSDs) varied from 2.2% to 9.4%, demonstrating that the reproducibility was acceptable.

4. Conclusions

In summary, a novel electrochemical biosensor was achieved for the detection of gliotoxin based on the MXene nanosheets and DN. In this work, MXene was served as a flexible and high-conductivity scaffold to conveniently immobilize a large number of DNs onto electrode surface, so the involved DNs are free of cumbersome modifications, thus significantly reducing assay's cost and operation difficulty. DNs were used as rigid scaffolds to support recognition elements for target binding. Combination of the benefits of two promising nanomaterials, the proposed sensor could detect gliotoxin as low as 5 pM in real samples and exhibited superior performance compared with previously developed sensors. The sensor for gliotoxin detection showed high selectivity, good reproducibility and acceptable stability. On the whole, this work opens a new avenue for mycotoxin detection using MXenes and DNs for clinical applications.

Funding

The authors declare that they have no known competing financial interests or personal relationships that could have appeared to influence the work reported in this paper.

CRediT authorship contribution statement

Hui Wang: Investigation, Visualization, Validation. **Hui Li:** Investigation, Data curation. **Yue Huang:** Resources. **Menghua Xiong:** Resources. **Feng Wang:** Writing - original draft, Supervision. **Chao Li:** Conceptualization, Methodology, Writing - review & editing, Supervision.

Acknowledgements

This work was supported by the National Natural Science Foundation of China (Grant 21804069, 81802978, and 31571023), the Distinguished Youth Foundation of Anhui Province (1808085J05), the Natural Sciences and Engineering Research Council of Canada and the Open Project of Key Laboratory of Biomedical Engineering of Guangdong Province (KLBEMGD201702).

Appendix A. Supplementary data

Supplementary data to this article can be found online at https://doi.org/10.1016/j.bios.2019.111531.

References

Brown, G.D., Denning, D.W., Gow, N.A.R., Levitz, S.M., Netea, M.G., White, T.C., 2012. Sci. Transl. Med. 4 (165), 165rv13.
Campuzano, S., Pedrero, M., Nikoleli, G.P., Pingarron, J.M., Nikolelis, D.P., 2017. Biosens. Bioelectron. 89, 269–279.
Cerqueira, L.B., de Francisco, T.M., Gasparetto, J.C., Campos, F.R., Pontarolo, R., 2014. PLoS One 9 (4), e92851.
Dillon, A.D., Ghidiu, M.J., Krick, A.L., Griggs, J., May, S.J., Gogotsi, Y., Barsoum, M.W., Fafarman, A.T., 2016. Adv. Funct. Mater. 26 (23), 4162–4168.
Eklund, P., Rosen, J., Persson, P.O.A., 2017. J. Phys. D Appl. Phys. 50 (11), 1361–6463.
Er, D., Li, J., Naguib, M., Gogotsi, Y., Shenoy, V.B., 2014. ACS Appl. Mater. Interfaces 6 (14), 11173–11179.
Gao, G., O'Mullane, A.P., Du, A., 2016. ACS Catal. 7 (1), 494–500.
Gao, S., Zheng, X., Tang, Y., Cheng, Y., Hu, X., Wu, J., 2019. Anal. Chem. 91 (2), 1610–1618.
Grovel, O., Kerzaon, I., Petit, K., Du Pont, T.R., Pouchus, Y.-F., 2006. J. Microbiol. Methods 66 (2), 286–293.
Han, X., Huang, J., Lin, H., Wang, Z., Li, P., Chen, Y., 2018. Adv. Healthc. Mater. 7 (9), 1701394.
Huang, R., He, N., Li, Z., 2018. Biosens. Bioelectron. 109, 27–34.
Kumar, S., Lei, Y., Alshareef, N.H., Quevedo-Lopez, M.A., Salama, K.N., 2018. Biosens. Bioelectron. 121, 243–249.
Lewis, R.E., Wiederhold, N.P., Chi, J., Han, X.Y., Komanduri, K.V., Kontoyiannis, D.P., Prince, R.A., 2005a. Infect. Immun. 73 (1), 635–637.
Lewis, R.E., Wiederhold, N.P., Lionakis, M.S., Prince, R.A., Kontoyiannis, D.P., 2005b. J. Clin. Microbiol. 43 (12), 6120–6122.
Li, C., Hu, X., Lu, J., Mao, X., Xiang, Y., Shu, Y., Li, G., 2018. Chem. Sci. 9 (4), 979–984.
Liu, B., Ma, L., Huang, Z., Hu, H., Wu, P., Liu, J., 2018. Mater. Horiz. 5 (1), 65–69.
Liu, F., Xu, Q., Huang, W., Zhang, Z., Xiang, G., Zhang, C., Liang, C., Lian, H., Peng, J., 2019. Electrochim. Acta 295, 615–623.
Naguib, M., Gogotsi, Y., 2014. Acc. Chem. Res. 48 (1), 128–135.
Novoselov, K.S., Geim, A.K., Morozov, S.V., Jiang, D., Zhang, Y., Dubonos, S.V., Grigorieva, I.V., Firsov, A.A., 2004. Science 306 (5696), 666–669.
Peng, J., Huang, Q., Liu, Y., Liu, P., Zhang, C., 2019. Sens. Actuators B Chem. 294, 157–165.
Peng, J., Huang, Q., Zhuge, W., Liu, Y., Zhang, C., Yang, W., Xiang, G., 2018. Biosens. Bioelectron. 106, 212–218.
Sang, X., Xie, Y., Lin, M.-W., Alhabeb, M., Van Aken, K.L., Gogotsi, Y., Kent, P.R., Xiao, K., Unocic, R.R., 2016. ACS Nano 10 (10), 9193–9200.
Sinha, A., Zhao, H., Huang, Y., Lu, X., Chen, J., Jain, R., 2018. Trac. Trends Anal. Chem. 105, 424–435.
Song, Y., Luo, Y., Zhu, C., Li, H., Du, D., Lin, Y., 2016. Biosens. Bioelectron. 76, 195–212.
Tiwari, J.N., Vij, V., Kemp, K.C., Kim, K.S., 2016. ACS Nano 10 (1), 46–80.
Wang, S.-F., Xie, F., Hu, R.-F., 2007. Sens. Actuators B Chem. 123 (1), 495–500.

Wen, Y., Rufford, T.E., Chen, X., Li, N., Lyu, M., Dai, L., Wang, L., 2017. Nano Energy 38, 368–376.
Wu, L., Lu, X., Wu, Z.-S., Dong, Y., Wang, X., Zheng, S., Chen, J., 2018. Biosens. Bioelectron. 107, 69–75.
Yang, F., Li, Q., Wang, L., Zhang, G.-J., Fan, C., 2018. ACS Sens. 3 (5), 903–919.
Yang, Y., Huang, Y., Li, C., 2019. Anal. Chim. Acta 1055, 90–97.
Yu, X., Cai, X., Cui, H., Lee, S.-W., Yu, X.-F., Liu, B., 2017. Nanoscale 9 (45), 17859–17864.